

Robust Adaptive Matched Filtering using the FRACTA Algorithm

KARL GERLACH, Fellow, IEEE

SHANNON D. BLUNT, Member, IEEE
Naval Research Laboratory

MICHAEL L. PICCIOLI, Senior Member, IEEE
SAIC

An effective method is developed for selecting sample snapshots for the training data used to compute the adaptive weights for an adaptive match filter (AMF); specifically a space/time adaptive processing (STAP) airborne radar configuration is considered. In addition, a new systematic robust adaptive algorithm is presented and evaluated against interference scenarios consisting of jamming, nonhomogeneous airborne clutter (generated by the Research Laboratory STAP (RLSTAP) or knowledge-aided sensor signal processing and expert reasoning (KASSPER) high-fidelity clutter models or using the multi-channel airborne radar measurement (MCARM) clutter data base), internal system noise, and outliers (which could take the form of targets themselves). The new algorithm arises from empirical studies of several combinations of performance metrics and processing configurations. For culling the training data, the generalized inner product (GIP) and adaptive power residue (APR) are examined. In addition two types of data processing methods are considered and evaluated: sliding window processing (SWP) and concurrent block processing (CBP). For SWP, a distinct adaptive weight is calculated for each cell-under-test (CUT) in a contiguous set of range cells. For one configuration of CBP, two distinct weights are calculated for a contiguous set of CUTs. For the CBP, the CUTs are in the initial training data and there are no guard cells associated with the CUT as there would be for SWP. Initial studies indicate that the combination of using the fast maximum likelihood (FML) algorithm, reiterative censoring, the APR metric, CBP, the two-weight method, and the adaptive coherence estimation (ACE) metric (we call this the FRACTA algorithm) provides a basis for effective detection of targets in nonhomogeneous interference. For the KASSPER data, FRACTA detects 154 out of 268 targets with one false alarm ($P_F \approx 3 \times 10^{-5}$) whereas the FML algorithm with SWP detects 11 with one false alarm. The clarvoyant processor (where each range cell's covariance matrix is known) detects 192 targets with one false alarm.

Manuscript received April 11, 2003; revised December 22, 2003; released for publication April 5, 2004.

IEEE Log No. T-AES/40/3/835889.

Refereeing of this contribution was handled by E. S. Chornoboy.

This work was supported by the Office of Naval Research (ONR 31) and Dr. Joseph Guerci of DARPA.

Authors' addresses: K. Gerlach and S. D. Blunt, Naval Research Laboratory, Code 5341, 4555 Overlook Ave., SW, Washington, D.C. 20375-5336, E-mail: (gerlach@radar.nrl.navy.mil); M. L. Picciolo, SAIC, 4501 Daly Dr., Suite 409, Chantilly, VA 20151-3707.

U.S. Government work not protected by U.S. copyright.

0018-9251/04/\$17.00 2004 IEEE

NOMENCLATURE

ACE	Adaptive coherence estimate
AMF	Adaptive matched filter
APR	Adaptive power residue
CBP	Concurrent block processing
CFAR	Constant false alarm rate
CTD	Censored training data
CUT	Cell-under-test
FML	Fast maximum likelihood algorithm
FRACTA	FML, reiterative censoring, APR metric, concurrent block processing, two weight method, adaptive coherence estimate (a combination of the above six methods)
GIP	Generalized inner product
ITD	Initial training data
KASSPER	Knowledge-aided sensor signal processing and expert reasoning
MCARM	Multi-channel airborne radar measurements
MLE	Maximum likelihood estimate
NB	Narrowband
RCFML/APR	Reiteratively censored fast maximum likelihood with adaptive power residue (metric) algorithm
RCFML/GIP	Reiteratively censored fast maximum likelihood with generalized inner product (metric) algorithm
RLSTAP	Research Laboratory space-time adaptive processor high-fidelity clutter model
STAP	Space-time adaptive processing
SWP	sliding window processing
UTD	Uncensored training data.

I. INTRODUCTION

Good performance for a class of multi-channel adaptive matched filters (AMF) requires the accurate estimation of the unknown input covariance matrix of the input channels. The true covariance matrix is used to find the optimal linear weighting of input sensors or channels such that the output signal-to-interference ratio is maximized. Due to this lack of knowledge of the external environment, adaptive techniques require a certain number of input data vectors (snapshots) to estimate effectively the input covariance matrix. In order to estimate the covariance matrix associated with a given snapshot, a group of snapshots in near proximity (in space and/or time) must be found which share (in some sense) the covariance matrix of a given snapshot. Normally for adaptive radar applications, the sample covariance matrix is estimated using training data from range cells close to the range cell-under-test (CUT). In the derivation of the maximum likelihood estimate (MLE) of the covariance matrix, it is normally assumed that the

CUT sample vector (the data vector to which the adaptive weight is applied) and all of the training data vectors are independent and identically distributed (IID). Such sample data are characterized as being homogeneous. In this work, we develop effective methods for selecting sample snapshots for the training data used to compute the adaptive weights for an AMF. Specifically, our interference scenario is related to the space/time adaptive processing (STAP) airborne radar configuration. We concern ourselves with the problem of estimating the covariance matrix when the input data vectors are 1) nonhomogeneous, 2) contain outliers, and 3) the CUT sample vector is in the training data.

There are a variety of conditions for which outlier data can be present. For example, unintentional temporally sporadic electromagnetic interference (EMI) could cause outliers, along with bad input sensor channels, or an intentional blinking interference source. These fluctuations in the input statistics could result in the covariance estimate of the external noise environment being severely misestimated which in turn results in degraded detection performance and an increase in the probability of false alarm. In addition, for the radar problem, sidelobe clutter discretes could be present in only a few range cells. The spatio-temporal covariance matrix of the sidelobe clutter discretes can be much different than say the surrounding clutter. This problem is closely related to the existence of land-sea clutter interfaces which cause significant degradation in airborne radar adaptive processing [1]. Also, power levels can be significantly different among the various patches of clutter. Another source of outlier data is the desired targets themselves. For example, if one is trying to detect an individual target adaptively in the presence of a formation of targets (such as an airborne formation), the other desired target returns located in distinct range cells about the individual desired target with essentially the same velocity vector can be present in the training data. All of the desired targets have approximately the same desired steering vector. The presence of the desired target returns in the training data can severely degrade the AMFs performance [2]. This is because the training data is used to estimate a weighting vector which is in the null space of the signal and interference sources that are in the training data. Hence, if a signal that has the desired signal's steering vector is in the training data, the adaptive weight vector may null the desired signal. In fact, this type of outlier, where the outlier has the same form as the desired signal vector, is a principal model for outliers that we use in our performance results. It was found that this type of outlier caused the most performance degradation of the "unrobustified" adaptive algorithms.

In [3], Gerlach developed a robust AMF whereby outlier data vectors in the training data were censored

from the covariance matrix estimate using the MLE setting. A reiterative censored fast maximum likelihood (RCFML) technique was presented which is based on eliminating a fixed number of snapshots from the training set in reiterative fashion using a version of the generalized inner product (GIP) [4] metric. The RCFML's convergence performance was shown to be relatively unaffected by the presence of outliers where the interference scenario consisted of homogeneous Gaussian noise plus the outliers. Other work [5–12] on nonhomogeneous AMF interference rejection is surveyed in [3]. Also see [23–25].

In addition to evaluating the RCFML developed in [3], we also evaluate a similar censoring method which uses the adaptive power residue (APR) metric as a discriminant for censoring sample snapshots. In its most simplistic form, the APR is the instantaneous power of the adaptive filter output for a range cell associated with a particular snapshot. The motivation for using the APR metric for censoring data samples is intuitively straightforward: a large APR (relatively speaking) would indicate that the given cell does not share all of the covariance matrix structure of the ambient cells and thus should be censored. A mathematical justification for using the APR is given in Section III.

We extend the methodology of [3] here by considering interference that results from the airborne radar STAP problem. For this scenario, the interference consists of nonhomogeneous airborne radar clutter, barrage jamming, receiver thermal noise, and outliers. The clutter was modeled using three mutually exclusive clutter data bases. Two of the clutter data bases were generated by clutter models: Research Laboratory STAP (RLSTAP) model [13] and the knowledge-aided sensor signal processing and expert reasoning (KASSPER) model [30] (a KASSPER challenge data cube was issued in April 2002 by DARPA and AFRL; we call this the KASSPER I data). These are high-fidelity airborne clutter generation models which produce site-specific airborne clutter radar data for the areas where the United States Geological Survey (USGS) digital terrain evaluation data (DTED) and land use cover (LULC) data are available. For the RLSTAP model, the nonhomogeneous terrain at White Sands, NM was chosen to provide representative nonhomogeneous land clutter for the more stressing radar scenarios where STAP is expected to be required for good performance. The KASSPER I data cube is a site-specific airborne radar scenario that addresses the ground moving target indicator (GMTI) problem in which the radar returns of several dense clusters of slow-moving (relative to the airborne platform) ground targets are buried in background land clutter. The terrain near Olancha, CA was chosen due to the nonhomogeneous land clutter from nearby mountains and deserts. The third clutter data base

is the multi-channel airborne radar measurements (MCARM) airborne radar data collected over the Delmarva peninsula [31].

Results are presented related to the performance of the APR and GIP censoring algorithms in a variety of interference scenarios and processing configurations. It is shown for representative examples that the APR is a more effective metric for identifying outliers than the GIP. In addition, a systematic approach for adaptively processing nonhomogeneous data which may contain outliers is presented. Initial studies indicate that the combination of using the fast maximum likelihood (FML) algorithm, reiterative censoring, the APR metric, concurrent block processing (CBP), the two-weight method, and the adaptive coherence estimation (ACE) metric (we call this the FRACTA algorithm) provides a basis for effective detection of targets in nonhomogeneous interference. This approach has the desirable feature of reducing the computational load by calculating one or two adaptive weights for a given block of input data rather than a distinct adaptive weight for each snapshot in a data block. A detailed description of the FRACTA algorithm is given in Section III.

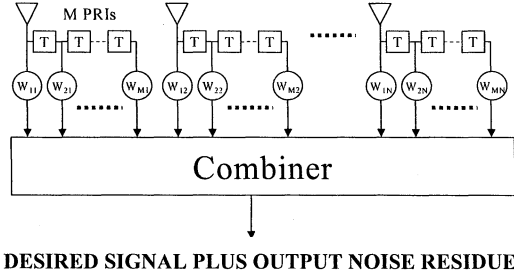
The RLSTAP clutter model and MCARM data are employed in different scenarios to evaluate the performance of the different metrics and processing configurations and thereby validate the algorithmic combination denoted as the FRACTA algorithm. The FRACTA algorithm is then applied to the KASSPER I challenge data cube whereby results associated with the detectability of ground targets for a given probability of false alarm are presented.

II. PRELIMINARIES

Consider a radar antenna system that consists of an N -element uniform linear array. The radar antenna system provides N RF input signals or channels. Time delayed inputs of these N inputs are to be combined via linear weighting to form an output such that an output performance measure (such as signal-to-noise (S/N) power ratio) is optimized. If the linear weighting is derived adaptively, such an implementation is called a STAP processor and is depicted in Fig. 1. Assume that for each of these RF channels, the radar frontend carries out amplification, filtering, reduction to baseband, and analog-to-digital (A/D) conversion. The output of each A/D is a data stream of in-phase and quadrature phase (I, Q) output pairs. The I and Q components represent the real and imaginary parts, respectively, of the complex valued data stream.

The radar waveform is assumed to be a burst of M identical pulses with pulse repetition interval (PRI) equal to T . Target detection is based upon the returns from this burst. The input data in the respective channels are sampled to form range-gate

N ELEMENT ANTENNA ARRAY



are statistically independent and with power equal to one. Thus $\bar{R}_t = I_M \otimes I_N$ where I_h denotes the h th order identity matrix and \otimes the Kronecker matrix product [14]. Furthermore it is commonly assumed that the jamming components are statistically independent from pulse to pulse (i.e. barrage jamming); thus it can be shown that $R_J = I_M \otimes R_J$ where R_J is the spatial $N \times N$ jamming covariance matrix associated with the elements of the linear array.

A data vector may contain a desired signal vector denoted by $a\mathbf{s}$ where a is an unknown complex amplitude and \mathbf{s} is an MN -length column vector related to the desired signal. For the input data structure previously described, the spatio-temporal steering vector \mathbf{s} takes the form:

$$\mathbf{s} = \mathbf{s}_d \otimes \mathbf{s}_s \quad (3)$$

where \mathbf{s}_d is an M -length temporal steering vector related to the desired signal's Doppler shift and \mathbf{s}_s is an N -length spatial steering vector associated with the desired signal's spatial phase shift. For a moving target with Doppler phase shift per pulse equal to ϕ : $\mathbf{s}_d = (1e^{j\phi} e^{2j\phi} \dots e^{(M-1)j\phi})^T$ where superscript T denotes transpose.

Given \mathbf{s} and the $MN \times MN$ interference covariance matrix \bar{R} , it is well known [29] that conjugate weighting of the MN -length primary data vector which maximizes the output signal-to-interference power ratio (SIR) is given by

$$\mathbf{w} = \bar{R}^{-1}\mathbf{s}. \quad (4)$$

For adaptive problems, \bar{R} is generally not known but we may have a priori information about the structure of \bar{R} . For example, previously we stated the jamming component of \bar{R} has the form $I_M \otimes R_J$ where R_J is the unknown $N \times N$ spatial jamming covariance matrix. Furthermore, for radar systems at microwave frequencies, the thermal noise is generally dominated by the internal noise power that can be readily measured. Hence, we assume that the thermal noise covariance matrix is known. Given this knowledge, we use the FML, [15, 16] algorithm to compute the adaptive weight from the training data.

The FML algorithm is used to estimate the unknown interference covariance matrix via MLE. Hence it was assumed that the unknown interference covariance matrix has the form of a known diagonal matrix (assumed to be the identity matrix) plus an unknown PSDH matrix. The FML convergence properties are similar to many of the fast converging techniques (such as loaded sample matrix inversion [20], eigen-projection [21, 22]; e.g. in a narrowband (NB) jamming scenario, convergence time (measured in the number of training snapshots necessary to attain an output signal-to-noise power performance that is 3 dB less than optimal) is on the order of twice the number of NB jammers [27, 28]. Furthermore, a

misestimation of the thermal noise level by as much as ± 10 dB does not significantly effect the FML's convergence performance [16]. The technique also works for any external interference environment, for example for wideband jammers and clutter without requiring modification.

In general, the covariance matrix \bar{R} will have to be estimated from a number of training data input vectors. Let K be the number of training data vectors. Normally for a given range CUT, the training data vectors used to calculate the adaptive weight are chosen to be associated with range indices that are in close proximity of the CUT range index. The motivation for choosing these indices is that it is highly likely that the training data and CUT will have approximately the same covariance matrix.

III. FRACTA DESCRIPTION

In this section we describe the last five components of the FRACTA algorithm (the FML algorithm was briefly discussed in the previous section). In addition, several alternative processing methods are discussed. First, methods are presented for censoring input data vectors from the training data. Let us define the initial training data (ITD) as an initial or original set of K input snapshots of length MN , the censored training data (CTD) as an K_{out} element subset of ITD of censored snapshots where K_{out} is a fixed number of input data vectors that are censored, and the uncensored training data (UTD) as the $K - K_{out}$ element subset of ITD of uncensored snapshots. Thus $ITD = UTD \cup CTD$. Let \mathbf{z}_k , $k = 1, 2, \dots, K$, denote the $MN \times 1$ vectors of ITD, and \tilde{R} equal the estimate of the covariance matrix which is derived using ITD.

There are two metrics that are most often used [1, 4, 6] to censor data vectors from the ITD. These are the GIP and the APR. For illustrative purposes (there are other ways of defining these metrics), these are defined by

$$GIP: \mathbf{z}'_k \tilde{R}^{-1} \mathbf{z}_k, \quad k = 1, 2, \dots, K \quad (5)$$

$$APR: |\mathbf{s}' \tilde{R}^{-1} \mathbf{z}_k|^2, \quad k = 1, 2, \dots, K. \quad (6)$$

The simplest form of a censoring algorithm using either one of the above metrics is as follows. Let m_k ($k = 1, \dots, K$) denote either $\mathbf{z}'_k \tilde{R}^{-1} \mathbf{z}_k$ or $|\mathbf{s}' \tilde{R}^{-1} \mathbf{z}_k|^2$. Let $m_{(k)}$, $k = 1, 2, \dots, K$ denote the ordered sequence where $m_{(1)} \leq m_{(2)} \leq \dots \leq m_{(K)}$. If K_{out} data vectors are to be censored, then the data vector indices corresponding to some combination of the K_{out} lowest and/or highest valued metrics are censored. The data vectors associated with the indices that were not censored are used to estimate the covariance matrix and hence to calculate the adaptive weight. For the censoring

algorithms to be presented, the highest valued metric indices are always censored.

Just as the GIP metric for outlier discrimination was derived in an approximate sense from an MLE setting [3], we now show that the APR metric can be derived under certain conditions in a similar fashion. The setup for demonstrating this is as follows. As mentioned previously, an outlier in the training data that is coaligned with the desired signal vector seems to cause the most significant performance degradation. Thus, let us assume that the outlier has steering vector \mathbf{s} . Assume that a given snapshot \mathbf{z}_k has a complex normal distribution denoted by $CN(0, R + c\mathbf{s}\mathbf{s}')$ were R is the interference covariance matrix (assumed known just for this derivation), and c is the unknown power of an outlier whose steering vector is \mathbf{s} . The likelihood function (LF) for \mathbf{z}_k is given by

$$LF(\mathbf{z}_k, a) = \frac{1}{\pi^{MN}} \frac{1}{|R + c\mathbf{s}\mathbf{s}'|} \exp\{-\mathbf{z}_k'(R + c\mathbf{s}\mathbf{s}')^{-1}\mathbf{z}_k\} \quad (7)$$

where $|\cdot|$ denotes determinant. The MLE solution for c is found by solving

$$c_{ML} = \arg \max_c LF(\mathbf{z}_k, c). \quad (8)$$

It is straightforward to show that

$$c_{ML} = \begin{cases} \left(\frac{|\mathbf{s}'R^{-1}\mathbf{z}_k|^2}{\mathbf{s}'R^{-1}\mathbf{s}} - 1 \right) \frac{1}{\mathbf{s}'R^{-1}\mathbf{s}} & \text{if } \frac{|\mathbf{s}'R^{-1}\mathbf{z}_k|^2}{\mathbf{s}'R^{-1}\mathbf{s}} > 1 \\ 0, & \text{otherwise.} \end{cases} \quad (9)$$

Thus in order to determine if the outlier is present, we check if c_{ML} is greater than some threshold τ , which is equivalent to checking if

$$|\mathbf{s}'R^{-1}\mathbf{z}_k|^2 > \tau' \quad (10)$$

where

$$\tau' = (\tau\mathbf{s}'R^{-1}\mathbf{s} + 1)(\mathbf{s}'R^{-1}\mathbf{s}) \quad (11)$$

and $|\mathbf{s}'R^{-1}\mathbf{z}_k|^2$ is the APR metric. Hence the APR metric results for this specific MLE setting.

An effective censoring methodology was introduced in [3], whereby data snapshots are censored reiterately. If Ω denotes the set of sample indices for a given ITD set, then it is evident that a reiterative procedure for eliminating an arbitrary number of data snapshot indices from Ω is to eliminate snapshots one at a time where at each step, Ω is set equal to the set of indices of the remaining snapshots. For example, if the APR metric were used, then on the first iteration the unknown covariance matrix would be estimated from the ITD using the FML. Thereafter, the APR metric is calculated for each of the K snapshots in the ITD (see (6)) and these are put in ascending order. The range sample snapshot associated with the largest APR is censored resulting in a new training data set that consists of the $K - 1$

remaining snapshots. The second iteration censors in similar fashion a snapshot from the remaining $K - 1$ snapshots where the unknown covariance matrix is calculated via the FML algorithm from these snapshots. This methodology is reiterated for as many times as desired. With respect to the GIP and APR metrics, we denote these censoring/adaptive weight technique as the reiterative censored FML using the GIP metric (or simply RCFML/GIP) and the reiterative censored FML using the APR metric (RCFML/APR).

In this work, we consider two methods of processing input data: standard sliding window processing (SWP) and concurrent block processing (CBP). For SWP, the CUT (a single range cell) and a fixed number of cells to the right and left of the CUT (these cells are called guard cells) are not in the ITD. In addition, the ITD changes for each CUT and consists of the $K/2$ (assume K is even) snapshots (indexed in range) to the immediate right of the right guard cells and $K/2$ snapshots to the immediate left of the left guard cells. The CUT has the center index of the ITD. An adaptive weight is calculated from the ITD or UTD (depending on whether censoring is used). This adaptive weight is applied just to the CUT. After a given CUT is adaptively processed, the next CUT (i.e., the CUT associated with the next contiguous range cell) is adaptively processed, and so on and so on. If SWP is used for the two censoring algorithms previously discussed, we designate these algorithms as SWP RCFML/GIP and SWP RCFML/APR. For CBP, there are no guard cells and the CUTs are a group of range indices centered on the center index of the ITD. One or two adaptive weights are calculated and applied back onto the CUTs. If CBP is used and one adaptive weight is calculated, we designate the previously mentioned censoring adaptive algorithms as CBP RCFML/GIP₁, and CBP RCFML/APR₁. A motivation for using CBP over SWP is the significant computational savings of computing one (or two) CBP adaptive weights for a block of CUTs versus computing a distinct SWP adaptive weight for every CUT in the block.

It was found via simulations that a two-weight CBP adaptive censoring algorithm yielded significantly better performance than the single-weight algorithm. For a single-weight algorithm, the adaptive weight is calculated from the UTD and applied to the ITD. For the two-weight algorithm, we calculate one weight from the ITD and apply it to the UTD; and calculate another weight from the UTD and apply it to the CTD. It was found for the single-weight algorithm that the average output noise power residue (no targets) associated with the uncensored range cells was considerably higher than the two-weight algorithm's average output noise power residue. Normally, the cells around a given CUT (and guard cells about the CUT) are used to establish the local

constant false alarm rate (CFAR) threshold. Hence a real target will stand higher above the local noise floor for the two-weight algorithm than the single-weight algorithm and thereby be more detectable. If CBP and the two-weight algorithm are used, we designate the previously mentioned censoring algorithms as CBP RCFML/GIP and CBP RCFML/APR (we suppress the subscript 2 on the GIP and APR for notational simplicity).

As a further measure of detectability, we use the Adaptive Coherence Estimate (ACE) [17, 18]. For a given range index k this is defined as

$$\text{ACE}(k) = \frac{|\mathbf{s}'\tilde{\mathbf{R}}_k^{-1}\mathbf{z}_k|^2}{(\mathbf{s}'\tilde{\mathbf{R}}_k^{-1}\mathbf{s})(\mathbf{z}'\tilde{\mathbf{R}}_k^{-1}\mathbf{z}_k)} \quad (12)$$

where $\tilde{\mathbf{R}}_k$ is the estimated covariance matrix for the k th range index. The ACE test statistic is often used in cascade with the CFAR test statistic in order to determine target detectability. The ACE screens out detections that are not closely coaligned with the desired steering vector \mathbf{s} , such as undernulled clutter or targets that are in the antenna/Doppler filter sidelobes. In essence, it is a signal correlation parameter which is normalized between 0 and 1.

The use of the ACE test statistic is highly motivated by the two-weight CBP adaptive censoring algorithm previously discussed. It was found that the APR of the range indices associated with the censored range indices (the ones that use the UTD to calculate the adaptive weight) was noticeably higher than the uncensored range indices (the ones that use the ITD to calculate the adaptive weight). Thus in some cases, a typical CFAR algorithm that averages the power of the cells about a given CUT might detect censored range indices that do not contain targets of interest (i.e., are not closely coaligned with the desired steering vector). Hence, a secondary test such as the ACE is necessary in order to screen these detections. In addition, the CFAR and ACE thresholds will have to be set accordingly in order to achieve a given probability of false alarm.

It was found that the combination of the two-weight CBP RCFML/APR test statistic and the ACE test statistic proved to be effective metrics for discerning real targets in nonhomogeneous interference. We call the combination of using the FML algorithm, reiterative censoring, the APR metric, CBP, the two-weight-method (2 adaptive weights) and the resultant ACE metric, the FRACTA algorithm where the first letter of each six components of the method is used to form the acronym.

A flowchart of the FRACTA algorithm is given in Fig. 2 (\mathbf{w}_U and \mathbf{w}_C denote the weight vectors for the uncensored and censored cells, respectively). The FRACTA algorithm operates as follows. APR censoring is applied to the ITD $\mathbf{z}_1, \mathbf{z}_2, \dots, \mathbf{z}_K$ such that the ITD is divided into UTD and CTD sets.

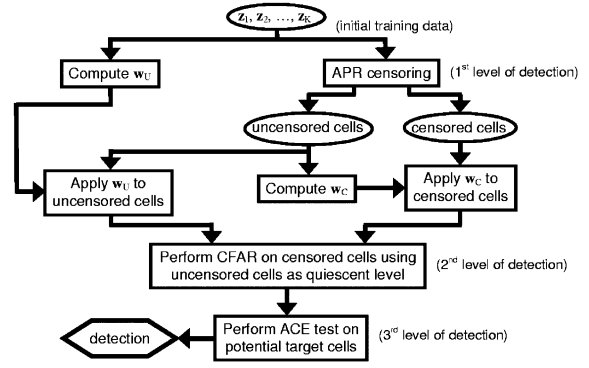


Fig. 2. FRACTA flowchart.

The UTD is used to compute the adaptive weight vector \mathbf{w}_C which is applied to the CTD to generate the censored output power residues. The ITD is used to compute the adaptive weight vector \mathbf{w}_U which is applied to the UTD to generate the uncensored output power residues. The censored output power residues are considered as CUTs for the local CFAR which uses the uncensored output power residues to estimate the quiescent local noise power level. The cells passing the CFAR detector are also tested with an ACE detector that compares the ACE test statistic of the respective candidate cells with some predetermined threshold. Cells that pass the ACE detector are declared as detections.

IV. RESULTS

In this section we first evaluate the effectiveness of different censoring metrics (e.g. GIP, APR) and processing configurations (e.g. SWP, CBP) using the RLSTAP clutter model and the MCARM data base. This is done in order to validate the various processing components of the FRACTA algorithm. We then apply the FRACTA algorithm to the KASSPER I challenge data cube. Results indicating the detectability of the simulated ground targets are presented. For the results to be shown, all power levels are normalized with respect to the internal noise power level which is set equal to 0 dB. Target powers are given as the integrated power level (integrated over antenna elements and pulses). Jammer and clutter power levels are given with respect to a given antenna element and pulse.

A. Preliminaries for RLSTAP Modeling

In this subsection, representative RLSTAP simulation results are presented which compare the performance of the various adaptive algorithms: SWP FML, SWP RCFML/GIP, SWP RCFML/APR, CBP FML, CBP RCFML/GIP, CBP RCFML/APR, and CBP RCFML/APR₁. The FML algorithm (using either SWP or CBP) was chosen as representative

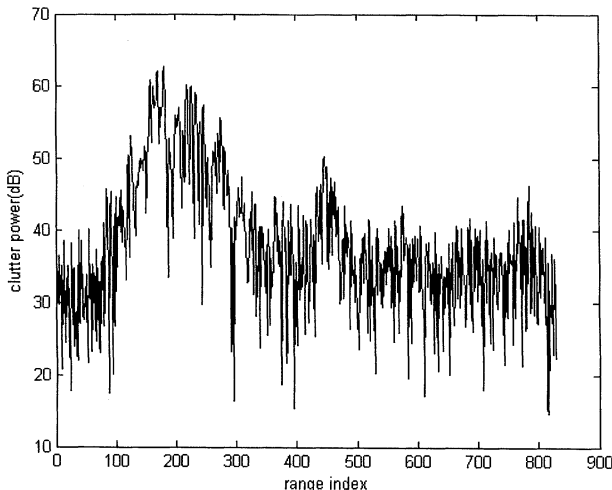


Fig. 3. Clutter power (dB) versus range index for RLSTAP data base.

of the variety of rank reduction techniques (e.g., LSMI, eigenprojection). The proposed algorithms were evaluated using a software clutter model called RLSTAP developed under a contract by the Air Force Research Laboratory (AFRL) in Rome, NY [13]. This software is a high fidelity airborne clutter generation model which produces site-specific airborne clutter radar data for the areas where the USGS DTED and LULC data are available. For this work, the nonhomogeneous terrain at White Sands, NM was chosen to provide representative nonhomogeneous land clutter for the more stressing radar scenarios where STAP is expected to be required for good performance. A plot of the clutter power (normalized to the internal power level) versus range index is shown in Fig. 3. From this plot, it is clear that the clutter power is nonhomogeneous and varies from 15–63 dB. The simulated radar was flying at 7000 m altitude at 250 m/s going true north, while operating at a UHF frequency of 435 MHz and transmitting a peak power of 140 kW. The 14 antenna array elements were spaced just less than a half-wavelength apart at 0.3331 m (0.97 half-wavelength spacing), and the antenna boresight was pointed exactly northwest, i.e., 45 deg from the direction of the platform velocity vector so as to point directly towards a nonfluctuating 10 square meter (radar cross section) moving target. The simulated airborne target velocity components were 100 m/s south and 100 m/s east (flying directly towards the radar along boresight), at an altitude of 2500 m, and at a distance of 70.7 km. The crab angle of the linear array was 315°. The pulse repetition frequency (PRF) was 625 Hz and there are 8 pulses per coherent processing interval (CPI). There are 829 range cells in the CPI to provide sample support for the adaptive processing.

We present plots of the APR or output power residue (after adaptive processing) versus the range index of the data for the various adaptive processing

methods. For the window of range indices shown on the plots, the interference consists of airborne clutter, barrage jamming, and internal noise at all ranges. In addition there are range-limited target(s) at various powers, range extents, and Doppler phases. The target(s) are always centered on the main beam of the radar antenna pattern. In previous studies [3, 23–25], it has been found that outliers that are almost coaligned with the desired signal vector cause the most significant degradation in adaptive processing performance. Hence, if the target(s) themselves are in the training data, these returns look like outliers. In fact, our outlier modeling will consist mostly of target-like returns in the ITD.

For the robust algorithms presented and evaluated, we arbitrarily chose the number of data snapshots to be censored (K_{out}). It is clear that a more effective procedure would be to develop an automatic stopping rule which estimates the number of outliers \hat{K}_{out} and sets the number of censored snapshots to \hat{K}_{out} plus an integer constant. This constant is chosen to ensure that with high probability (to be chosen) K_{out} is greater than the true number of outliers. The development of an effective stopping rule is left as a topic of future research.

For the representative RLSTAP performance plots to be shown, the snapshot length is (number of antenna elements) \times (number of pulses) = 14 \times 8 = 112. It was found via simulation (not shown) that about 80 snapshots in the ITD was sufficient in order to obtain good clutter and jamming rejection for the algorithms to be compared for the no outliers case. Targets, jamming, and internal noise are added to the RLSTAP clutter data base. The clutter power level (normalized to the internal noise level) for the various range indices is indicated in Fig. 3. The simulated target(s) have a Doppler phase shift of 171° and the β -parameter [26] (the number of half-wavelength spacings traversed by the airborne radar platform during a PRI) is 2.73. The β -parameter is directly related to the effective rank of the clutter covariance matrix. Finally, the number of sample snapshots censored from the ITD, K_{out} , is set equal to 20. This number was chosen to be slightly greater than the maximum number of added outliers in the ITD. The resultant number of snapshots in the CTD will be 60 which is still sufficient in order to attain good interference rejection in the presence of no outliers.

B. RLSTAP SWP Results

Performance results for SWP are shown in Figs. 4–7. For the SWP the number of guard cells used is six (three on each side of the CUT). For these figures (and Figs. 4–21 except Fig. 19), there are two 30 dB jammers (along with the other interference). In Figs. 4 and 5, there is a single 35 dB target centered

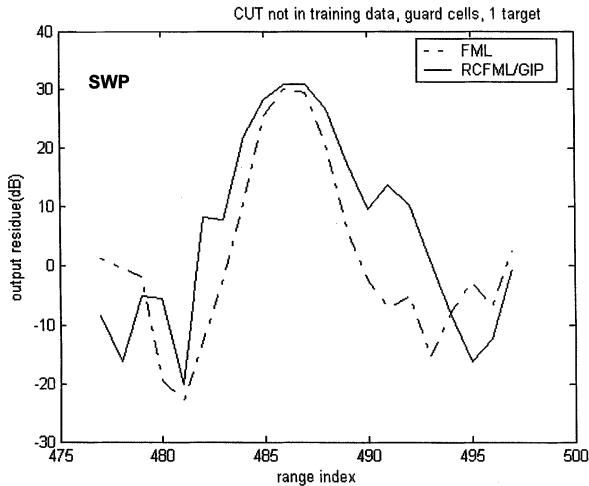


Fig. 4. APR versus range index for SWP FML and SWP RCFML/GIP algorithms, 1 target, RLSTAP.

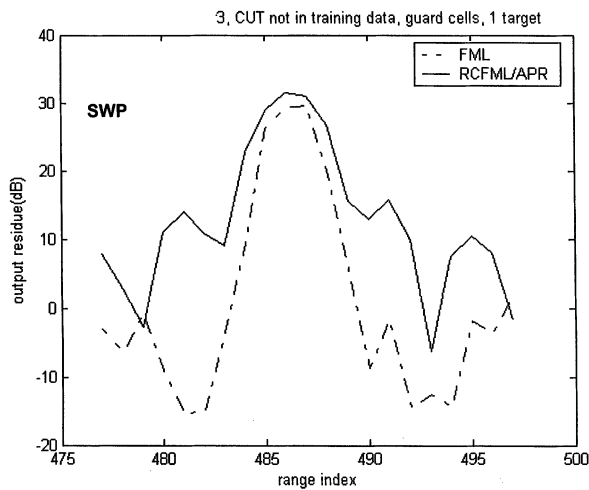


Fig. 5. APR versus range index for SWP FML and SWP RCFML/APR algorithms, 1 target, RLSTAP.

at range index 487 with range extent equal to 7. The relative performances of the SWP RCFML/GIP (we suppress the SWP in the figure legend) versus the FML and the SWP RCFML/APR versus the FML can be viewed in Figs. 4 and 5, respectively. For this single target example, it is clear that the FML outperforms the censoring algorithms and that the SWP RCFML/GIP is slightly better than the SWP RCFML/APR.

We now examine the effect of two spatially distinct targets on the adaptive algorithm's performance. For Figs. 6 and 7, the set-up is identical to Figs. 4 and 5 except a second target of power 30 dB is centered a range index 480 and has range extent equal to 3. From Figs. 6 and 7, it is seen that the FML algorithm's performance has significantly degraded (relative to the one target case). Furthermore, in terms of target detection, the SWP RCFML/APR reveals the range extent of the second target whereas the SWP RCFML/GIP does not. However, the range sidelobes

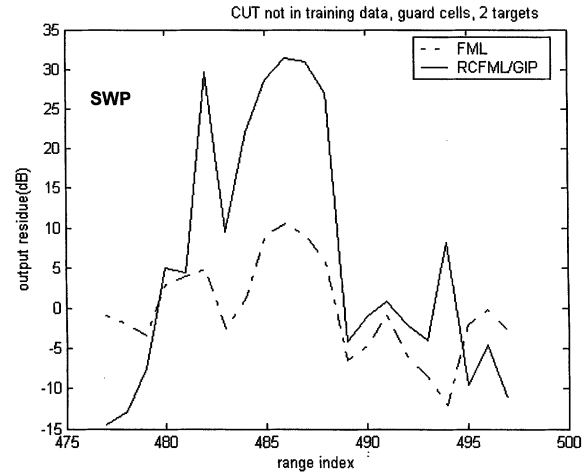


Fig. 6. APR versus range index for SWP FML and SWP RCFML/GIP algorithms, 2 targets, RLSTAP.

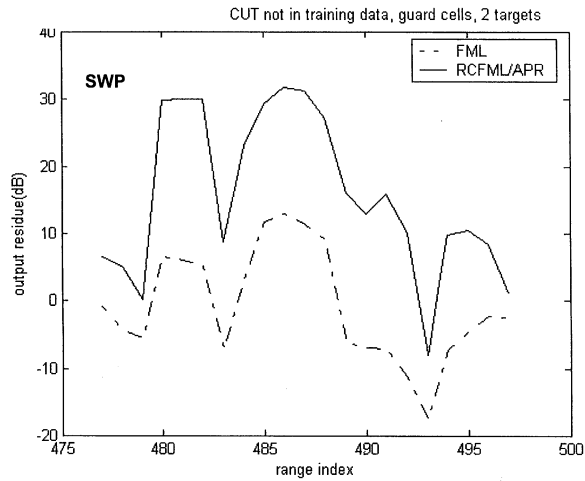


Fig. 7. APR versus range index for SWP FML and SWP RCFML/APR algorithms, 2 targets, RLSTAP.

(where targets are not present) are higher (by about 5 dB) for the SWP RCFML/APR than the SWP RCFML/GIP.

C. RLSTAP CBP Results

For the rest of the RLSTAP figures, we consider exclusively CBP which was discussed in Section III. Thus there are no guard cells and all target returns are in the ITD. Besides showing the APR measure in the figures, we plot the ACE*10 metric and show which range indices are censored. This is accomplished by plotting the indicator function, CENSOR (k), where CENSOR (k) = 5, if the snapshot associated with range index k is censored, and CENSOR (k) = 0, if it is not censored.

For Figs. 8–21 (except Fig. 12), two-weight adaptive censoring algorithms are used (i.e., CBP RCFML/APR or CBP RCFML/GIP). For notational simplicity, we suppress the CBP designation in the figure legend. For Figs. 8 and 9, we use the same

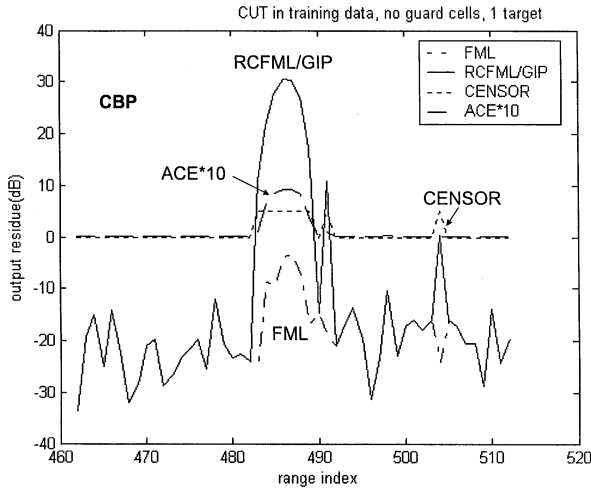


Fig. 8. APR versus range index for CBP FML and CBP RCFML/GIP algorithms, 1 target, RLSTAP.

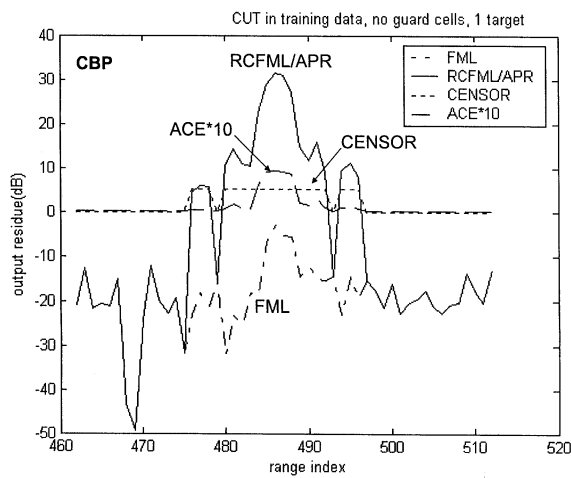


Fig. 9. APR versus range index for the CBP FML and CBP RCFML/APR algorithms, 1 target, RLSTAP.

target and interference scenario as Figs. 4 and 5. There is one target centered at range index 487 and it has extent equal to 7. From these figures, it is clear that the adaptive censoring algorithms are superior to the FML. Also comparing Figs. 8 and 9 with Figs. 4 and 5, CBP is superior to SWP. It is seen from these figures as noted previously, that the censored data indices' APRs are noticeably higher than the noncensored data indices' APRs. However, if these were detected via a local cell-averaging CFAR test (where censored samples are not included in the averaging which is used to estimate the local power level), then the ACE test (as indicated by the ACE*10 metric in the figures), would most likely screen out these detections.

For Figs. 10 and 11, we use the same target and interference as Figs. 6 and 7. There are two targets. It is clear from these two figures that the CBP RCFML/APR algorithm is superior to the CBP RCFML/GIP. In fact for a number of simulation

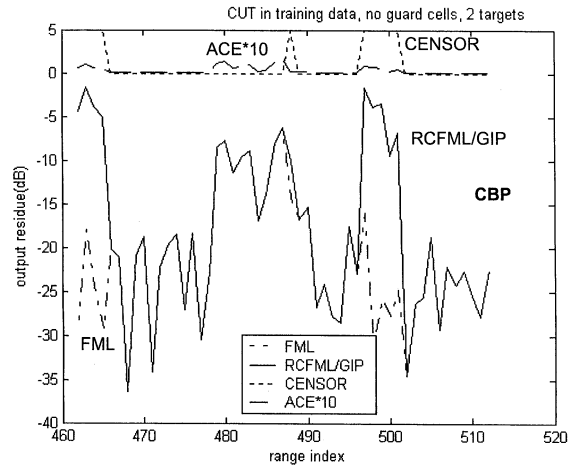


Fig. 10. APR versus range index for CBP FML and CBP RCFML/GIP algorithms, 2 targets, RLSTAP.

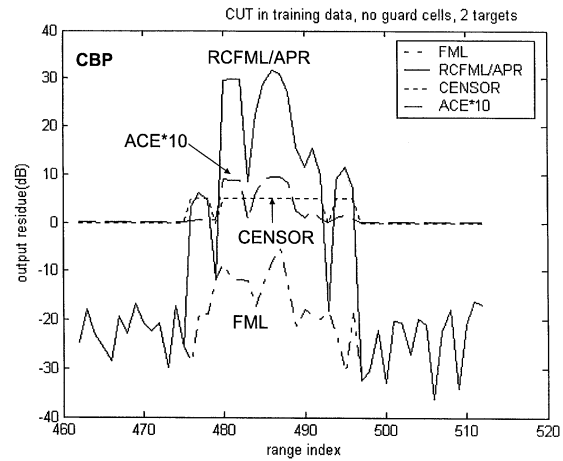


Fig. 11. APR versus range index for CBP FML and CBP RCFML/APR algorithms, 2 targets, RLSTAP.

results (not shown), the CBP RCFML/APR was much more robust than the CBP RCFML/GIP. A possible explanation for the discrimination superiority of the APR metric to the GIP metric can be found by examining their forms given by Eqs. (5) and (6). If we define $\mathbf{u}_k \equiv \tilde{R}^{-1/2} \mathbf{z}_k$ and $\mathbf{s}_0 \equiv \tilde{R}^{-1/2} \mathbf{s}$, then for the GIP, the test statistic equals $|\mathbf{u}_k' \mathbf{u}_k|^2$ which is a noncoherent integrator form, and for the APR, the test statistic equals $|\mathbf{s}_0' \mathbf{u}_k|^2$ which is a coherent integrator form. From detection theory (see e.g. [19, p. 391]), we know under certain conditions, for a given false alarm probability and signal-to-noise ratio that the detection probability for a coherent integrator test statistic is greater than that of a noncoherent integrator test statistic. This would imply that the APR metric is better at detecting/censoring outliers than the GIP metric.

For Fig. 12, the target and interference scenario is identical to Fig. 11, except we use the single-weight censoring algorithm, CBP RCFML/APR₁. From this figure (and other simulations not shown), it

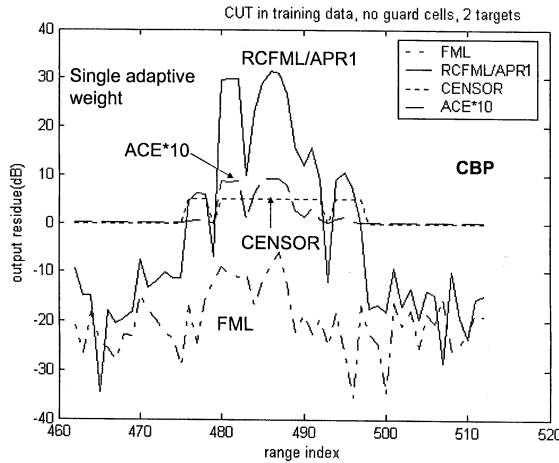


Fig. 12. APR versus range index for CBP FML and CBP RCFML/APR₁ (single weight) algorithms, 2 targets, RLSTAP.

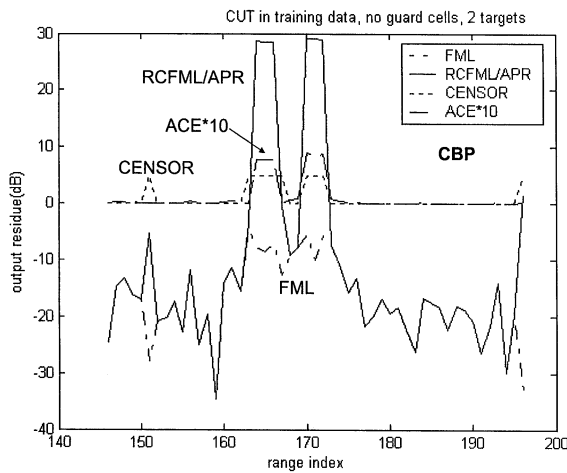


Fig. 13. APR versus range index for CBP FML and CBP RCFML/APR algorithms. Two targets located about range index 170, RLSTAP.

is seen that the range sidelobe noise floor rises significantly (10 dB) when a single-weight algorithm is used. Hence the two-weight adaptive censoring algorithm has markedly better performance than the single-weight algorithm.

For Fig. 13, we show performance results for when there are two targets, two jammers, and the targets are located at range indices 164 and 171. Both targets have range extent equal to 3. Referring to Fig. 3, it is seen that the instantaneous clutter power varies from 45 dB to 65 dB (i.e., the power level is large and highly nonhomogeneous) across the 80 range indices that are used in the ITD. From Fig. 13, it is seen that the two targets are easily discernible.

For the results shown in Fig. 8–13, the ITD was centered at range index 487. Hence the ITD was roughly centered about where the two targets were placed for the target scenarios presented. We wish to determine the effects on performance when the center index of ITD is considerably different than

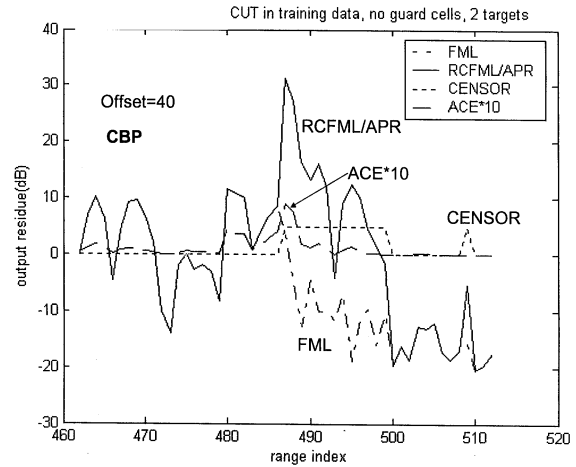


Fig. 14. APR versus range index for CBP FML and CBP RCFML/APR algorithms. Two targets. Adaptive weight calculation range index offset = 40, RLSTAP.

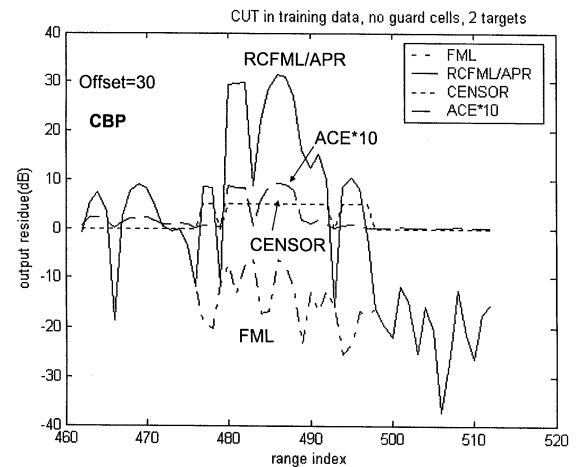


Fig. 15. APR versus range index for CBP FML and CBP RCFML/APR algorithms. Two targets. Adaptive weight calculation range index offset = 30, RLSTAP.

the range indices where targets and/or outliers reside. For Figs. 14–16, the range index where the ITD is centered is varied by an offset from range index 487. On the figures this is indicated by the parameter, offset. For Figs. 14, 15, and 16 the offset is 40, 30, and 20, respectively (e.g. an offset = 40 indicates that the ITD is centered at range index, $487 - 40 = 447$), and the target/interference scenario is identical to Fig. 9. An offset of 40 places the target centered at range index 487 at the very edge of the data indices contained in the ITD. From Fig. 14 (offset = 40), it is clear that performance degrades significantly; the target at range index 487 is discernable but its extent is not. The target at range index 480 is no longer discernable. From Fig. 15 (offset = 30), the two targets and their range extent is discernable but the range sidelobe level is significantly degraded (as compared with Fig. 9). For Fig. 16 (offset = 20), the performance is very close to when the offset = 0. Thus for this representative example, it would seem that

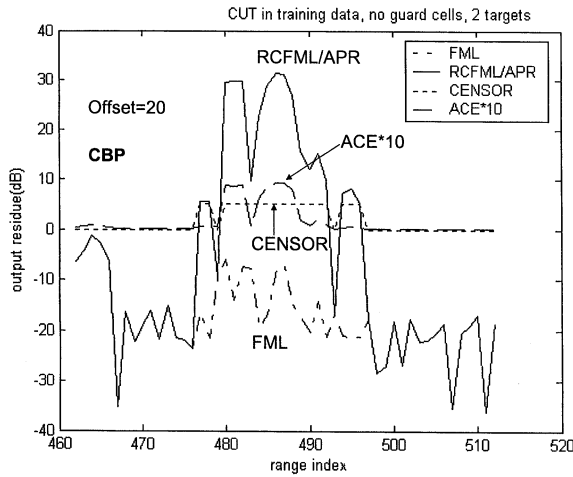


Fig. 16. APR versus range index for CBP FML and CBP RCFML/APR algorithms. Two targets. Adaptive weight calculation range index offset = 20, RLSTAP.

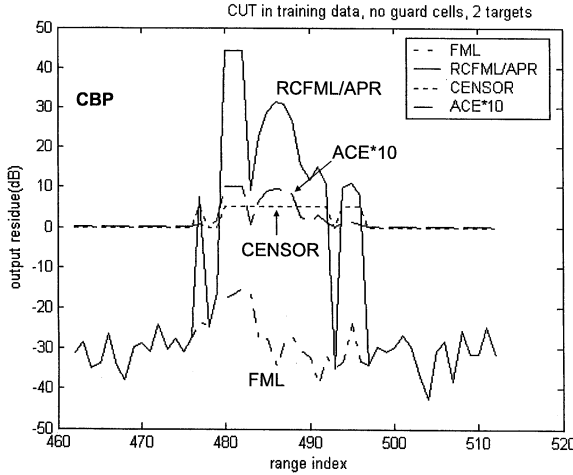


Fig. 17. APR versus range index for CBP FML and CBP RCFML algorithms. Two targets; target powers = (30 dB, 45 dB), RLSTAP.

the CUT's block length (i.e., the number of range indices to which the two adaptive weights derived from a single ITD would be applied) is 40. Thus for a contiguous set of range indices being processed, there would be a 50% overlap in the indices associated with the successive ITDs. As a result the CBP adaptive censoring methods would require 1/40th of the computations used by the SWP adaptive censoring methods for the interference scenarios presented.

For Figs. 17 and 18, the target/interference scenario is identical to Fig. 9 (2 targets) except the power of the target at range index 480 is varied: 45 dB in Fig. 17 and 15 dB in Fig. 18. From the two figures, the targets are readily discernable using the APR and ACE metrics.

For Fig. 19, the target/interference scenarios is identical to Fig. 9 (2 targets) except the number of 30 dB sidelobe jammers is four. Performance is similar to the two jammer case shown in Fig. 19.

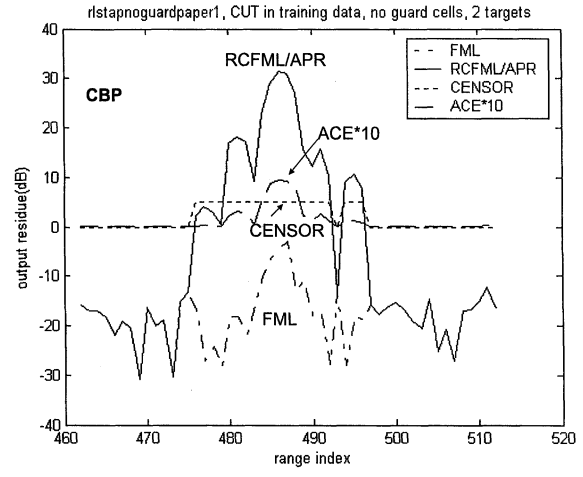


Fig. 18. APR versus range index for CBP/FML and CBP RCFML/APR algorithms. Two targets; target powers = (30 dB, 15 dB), RLSTAP.

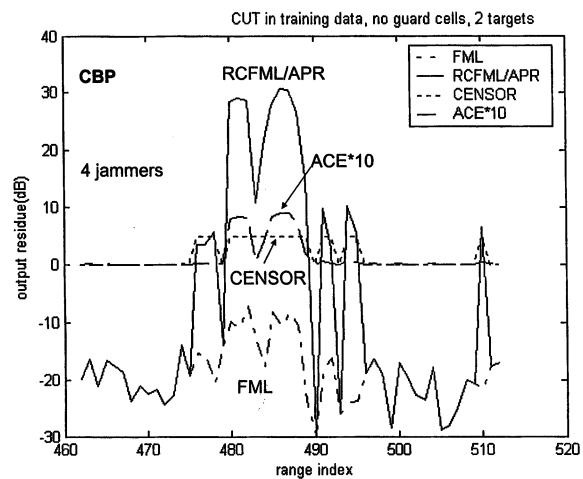


Fig. 19. APR versus range index for CBP FML and CBP RCFML/APR algorithms. Two targets. Four jammers, RLSTAP.

For Figs. 20 and 21, the target/interference scenario is identical to Fig. 9 (2 targets) except, we have injected 30 dB target/outliers every fifth range index. All target/outliers are at the center of the radar antenna main beam. For Fig. 20, the injected targets/outliers Doppler phase is random; each chosen from a uniform distribution on: $(-40^\circ, 40^\circ)$. For this figure, it is seen that the injected target/outliers are not discernable using the combined APR/ACE metrics. At some range indices where the off-Doppler target/outliers reside, the APR metric is high when compared with the surrounding range indices, but the ACE metric is very small indicating the absence of a target sharing the desired signal's steering vector. For Fig. 21, the injected targets' (outliers) Dopplers is random, each chosen from a uniform distribution: $(170.9^\circ, 171.1^\circ)$. Hence the injected targets/outliers' steering vector is close to the desired signal's. From Fig. 21, it is seen that all of the injected target/outliers

TABLE I
Summary of Results using RLSTAP Data Base Against Various Configurations/Scenarios

Fig.	Config.	Proc.	Number of Targets	Target Power dB	Picket Fence/ Dopp. Offset	Range Offset	Number of Jammers	Jammer's Power dB	Range Window Center	Conf. P/S dB Targets 1, 2	Conf. P/S dB Targets 1, 2	FML P/S dB Targets 1, 2
4	RCFML/GIP	SWP	1	32	No	NA	2	30	487	32	NA	32
5	RCFML/APR	SWP	1	32	No	NA	2	30	487	25	NA	32
6	RCFML/GIP	SWP	2	32, 33	No	NA	2	30	487	30, 27	NA	10, 5
7	RCFML/APR	SWP	2	32, 32	No	NA	2	30	487	25, 25	NA	10, 5
8	RCFML/GIP	CBP	1	32	No	0	2	30	487	40	.9	10
9	RCFML/APR	CBP	1	32	No	0	2	30	487	43	.9	10
10	RCFML/GIP	CBP	2	32	No	0	2	30	487	18, 16	.1, .1	10, 7
11	RCFML/APR	CBP	2	32	No	0	2	30	487	45, 42	.9, .8	10, 7
12	RCFML/APR1	CBP	2	32	No	0	2	30	487	38, 35	.9, .8	10, 7
13	RCFML/APR	CBP	2	32	No	0	2	30	171	38, 37	.9, .8	10, 10
14	RCFML/APR	CBP	2	32	No	40	2	30	487	20, 7	.8, .3	0, 10
15	RCFML/APR	CBP	2	32	No	30	2	30	487	20, 18	.9, .8	5, 5
16	RCFML/APR	CBP	2	32	No	20	2	30	487	40, 37	.9, .8	5, 5
17	RCFML/APR	CBP	2	32, 47	No	0	2	30	487	55, 70	.9, 1.	0, 10
18	RCFML/APR	CBP	2	32, 15	No	0	2	30	487	45, 30	.9, .3	10, 0
19	RCFML/APR	CBP	2	32, 32	No	0	4	30	487	45, 42	.9, .8	5, 5
20	RCFML/APR	CBP	2	32, 32	Yes, $\pm 40^\circ$	0	2	30	487	45, 42	.9, .8	8, 5
21	RCFML/APR	CBP	2	32, 32	Yes, 0°	0	2	30	487	50, 50	.8, .8	5, 7

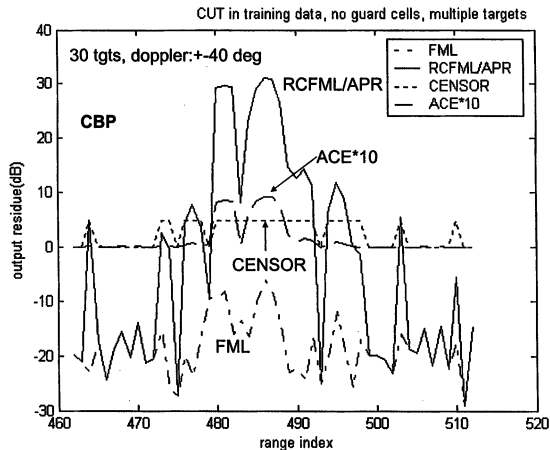


Fig. 20. APR versus range index for CBP FML and CBP RCFML/APR algorithms. Two targets and mismatched targets ($\pm 40^\circ$ Doppler) placed every fifth range index, RLSTAP.

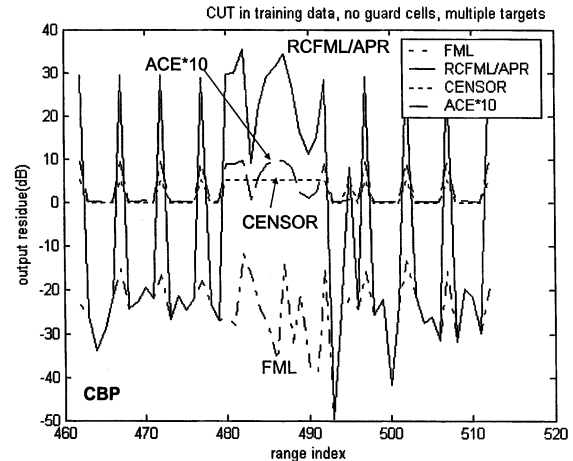


Fig. 21. APR versus range index for CBP FML and CBP RCFML/APR algorithms. Two targets and matched targets (171° Doppler) placed every fifth range cell, RLSTAP.

and the two targets located at cell indices 487 and 488 are discernable by the APR and ACE metrics.

A summary of results using the RLSTAP data base against various configurations and interference scenarios is given in Table I. The metric, peak target power to range average sidelobe power (P/S), is given in the table as a measure of processor configuration performance. In addition the ACE metric is shown. The higher these performance metrics, the better that a processing configuration is performing. For comparison, the FML P/S for a given setup is

shown. The results from this table clearly highlight the benefits of using the algorithmic components embodied by the FRACTA algorithm.

D. MCARM Results

In this subsection, results related to evaluating components of the FRACTA algorithm against the MCARM clutter data base are presented. The MCARM airborne radar data was collected on a BAC 1-11 jet aircraft with a sidemounted planar array

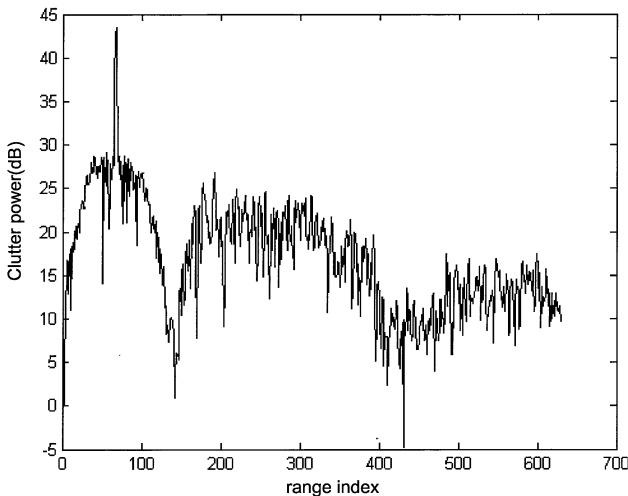


Fig. 22. Clutter power (dB) versus range index for MCARM data base.

operating at L-band with a linear frequency modulated (LFM) pulsed waveform. It provides $0.8 \mu\text{s}$ range resolution (i.e., 120 m) using a 0.8 MHz receiver bandwidth and the transmit pattern beamwidth is 7.5 deg. The array is composed of 2 rows of 11 elements each. Each vertical pair of elements is joined by a fixed network that acts to sharpen the elevation beamwidth providing a nominal amount of vertical array gain and the vertical pattern is pointed (mechanically) down (i.e., -5.4 deg from level flight). The output of 11 element pairs (i.e., 11 subarrays spaced 1/2 wavelength apart) in azimuth are each connected to separate receivers, balanced, superheterodyned, and sampled at a 5 MHz sampling rate in the IF stage. The PRF is 1984 Hz corresponding to 630 unambiguous range cells out to 40.82 nmi. Data was taken over the Delmarva Peninsula near the eastern shore of Maryland in 1995–1996 timeframe. The MCARM jet flew south while the transmit beam pointed east towards the eastern shore of Maryland and returned ground clutter and any moving targets of opportunity. The MCARM jet had an altitude of 7600 ft with a ground speed of 427.7 knots. The roll, pitch, and crab angles were -7.5 deg, 4.13 deg, and 4.7 deg, respectively, where the crab angle is defined to be the angle between the velocity vector of the radar antenna array and the antenna array axis.

The clutter power versus range profile for the MCARM data is shown in Fig. 22. The first 150 range indices are contaminated with transmit power leakage and are not used. Our interference model consists solely of the MCARM data (no jamming was injected). Targets are added to the MCARM clutter data base. Results are shown for three cases: two 20 dB range spread targets (each over 3 range indices) are injected at 1) range indices 293, 300, 2) range indices 393, 400, and 3) range indices 493, 500.

These cases put multiple targets in the middle of the Delmarva (case 1) and either side of the Delaware River (case 2 and 3, range indices 400–475 are associated with the Delaware River). The latter cases are associated with processing across the land/river interface which results in nonhomogenous clutter samples.

For the representative performance plots to be shown, the snapshot length is $(\text{number of antenna elements}) \times (\text{no. pulse}) = 11 \times 8 = 88$. It was found via simulation (not shown) that about 120 snapshots in the ITD was sufficient in order to obtain good clutter and jamming rejection for the algorithms to be compared when no outliers were present. The simulated targets have a Doppler phase shift of 90°. Finally, the number of sample snapshots censored from the ITD, K_{out} , is set equal to 20.

Results for the three cases are shown in Figs. 23–25. In these figures, APR is shown for the two processing configurations: CBP FML and CBP RCFML/APR. In addition the censoring indicator, CENSOR, and the ACE*10 metric is shown for the CBP and RCFML/APR. Clearly the output residue curves and the ACE*10 metric indicate the presence and range extent of the injected targets when using the CBP RCFML/ACE processing configurations for the three cases.

E. Results for KASSPER Modeling

In this subsection, simulation results are presented for the KASSPER I challenge data cube when employing the standard SWP FML algorithm and the FRACTA algorithm. The KASSPER I data cube is simulated high-fidelity airborne radar data for the nonhomogeneous terrain near Olancha, CA that consists of mountains and deserts. A plot of the clutter power versus range index is shown in Fig. 26 in which the peaks and troughs are most likely a result of shadowing due to mountains. The simulated radar was flying at 3000 m altitude at 100 m/s going due east (270° measured from true north) with a 3° crab angle. The radar was operating at 1240 MHz with a peak power of 15 kW. The 11 (virtual) antenna array elements were spaced slightly less than a half-wavelength apart at 0.1092 m (0.9028 half-wavelength spacing), and the antenna boresight was pointed at 177°. The PRF was 1984 Hz and 32 pulses per CPI were generated. There were 1000 range cells of data generated covering 35 km to 50 km.

There were 268 ground traffic targets within the beam of the radar. The targets were classified into two general classes: military-like target clusters and background traffic. The background traffic were placed randomly on the existing roads. The target clusters were densely spaced groups of vehicles placed on several chosen roadways. Both classes of targets have a complex scattering amplitude

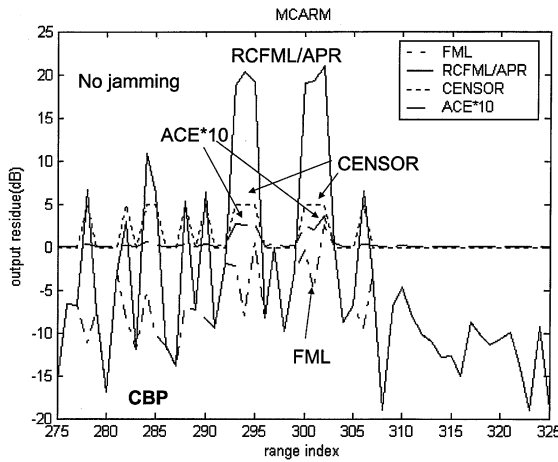


Fig. 23. APR versus range index for CBP FML and CBP RCFML/APR algorithms, 2 targets, targets at 293 and 300, MCARM.

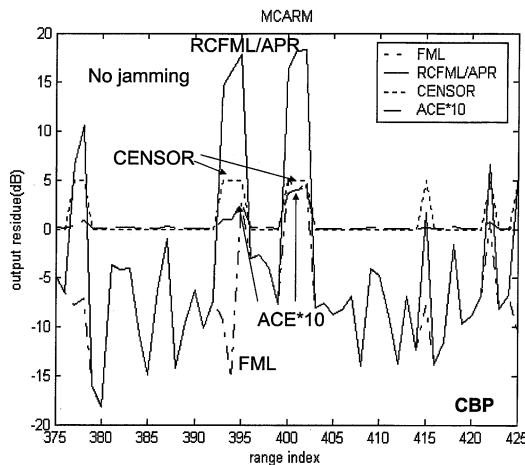


Fig. 24. APR versus range index for CBP FML and CBP RCFML/APR algorithms, targets at 393 and 400, MCARM.

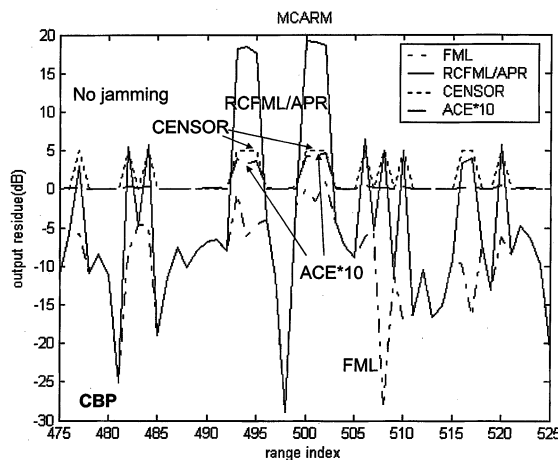


Fig. 25. APR versus range index for CBP FML and CBP RCFML/APR algorithms, targets at 493 and 500 MCARM.

that is drawn from a zero-mean complex Gaussian distribution with variance equal to either 5 or 15 dBsm average radar cross section. Furthermore,

the KASSPER scenario contains stationary man-made clutter discretes such as buildings and towers (TV/radio) that further compound the nonhomogeneity of the clutter returns.

Each snapshot has 11 antenna elements \times 32 pulses = 352. We designate the size of the ITD blocks to be $K = 150$ snapshots from which $K_{\text{out}} = 20$ are censored. The resulting number of snapshots, 130, is slightly more than twice the number of dominant eigenvalues of the sample covariance matrix for the KASSPER model and therefore is sufficient to attain good interference rejection [16, 27, 28]. Detection performance is based upon the number of correct detections for a single false alarm which results in a estimated probability of false alarm of $1/(32 \times 1000) = 3.125 \times 10^{-5}$.

Performance results for FRACTA when applied to the KASSPER challenge data cube are shown in Fig. 27 which plots the true targets (black x) and the detections (gray bar) as a function of Doppler bin (in m/s) and range (in km) (the width of the gray bar is 17 m/s which is the resolution of a Doppler filter). For a single false alarm the FRACTA algorithm correctly detected 154 out of the 268 targets present. This compared well with the 192 out of 268 detected when clairvoyant knowledge of the clutter covariance matrices are available and was considerably better than the standard SWP FML processor which detected 11 of the 268 targets (again, one false alarm). When the ACE detection was cascaded with the SWP FML detector, 65 of the 268 targets were detected.

V. CONCLUSIONS

An effective method was developed for selecting sample snapshots for the training data used to compute the adaptive weights for an AMF; specifically a STAP airborne radar configuration was considered. In addition, a new systematic robust adaptive algorithm was presented and evaluated against interference scenarios consisting of jamming, nonhomogeneous airborne clutter internal system noise, and outliers (which could take the form of targets themselves). For culling the training data, the GIP and APR were examined. In addition two types of data processing methods were considered and evaluated: SWP and CBP. For SWP, a distinct adaptive weight was calculated for each CUT in a contiguous set of range cells. For one configuration of CBP, two distinct weights were calculated for a contiguous set of CUTs. For the CBP, the CUTs were in the initial training data and there are no guard cells associated with the CUT as there would be for SWP. Initial studies indicated that the combination of using the FML algorithm, reiterative censoring, the APR metric, CBP, the two-weight method, and the ACE metric (we call this the FRACTA algorithm) provides a basis for effective detection of targets in nonhomogeneous interference.

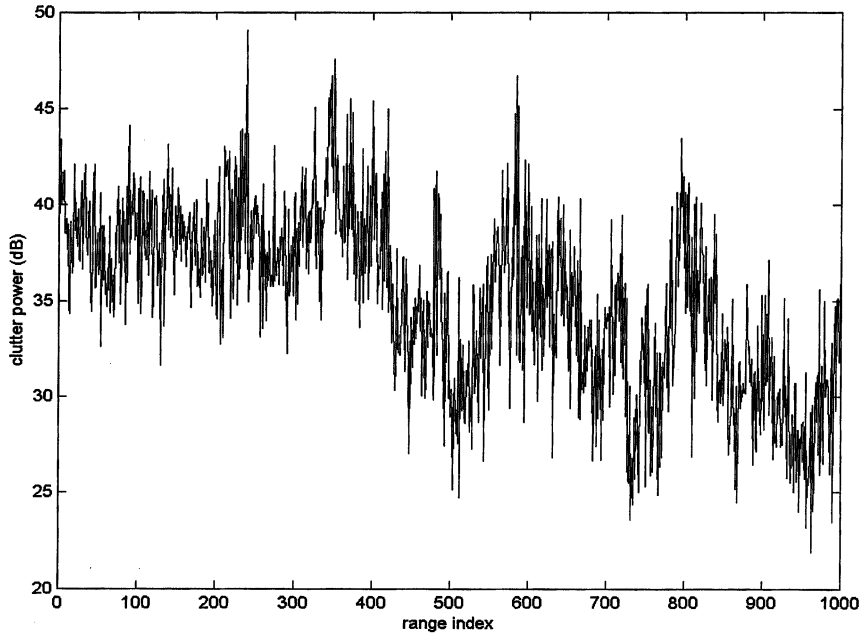


Fig. 26. Clutter power (dB) versus range index for KASSPER I data cube.

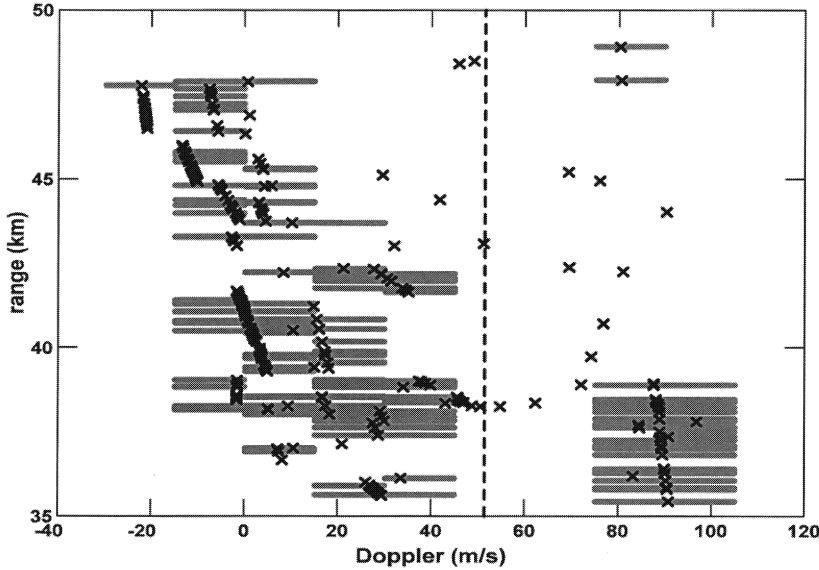


Fig. 27. Detection performance of FRACTA, KASSPER I.

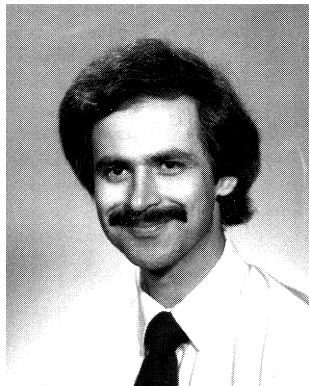
The FRACTA algorithm arose from empirical studies of several performance metrics and processing configurations. The clutter was generated using three mutually exclusive data bases: RLSTAP, MCARM, and KASSPER. The RLSTAP and MCARM data were employed in different scenarios to evaluate the different performance metrics and processing configurations and thereby validate the combination of methods denoted as the FRACTA algorithm. The total FRACTA algorithm was used on the KASSPER I data cube to evaluate detection performance. For this data, it was found that FRACTA detected 154 out of 268 targets with one false alarm ($P_F \approx 3 \times 10^{-5}$) whereas the FML algorithm with SWP detected 11 for the same P_F . The clarvoyant processor (where each range

cell's covariance matrix is assumed known) detected 192 targets with one false alarm.

REFERENCES

- [1] Adve, R. S., Hale, T. B., and Wicks, M. C. (2000) Practical joint domain localized adaptive processing homogeneous and nonhomogeneous environment, Part 2: Nonhomogeneous environments. *IEE Proceedings, Radar, Sonar Navigation*, **147**, 2 (Apr. 2000), 66–74.
- [2] Gerlach, K. (1995) The effects of signal contamination on two adaptive detectors. *IEEE Transactions on Aerospace and Electronic Systems*, **30**, 1 (Jan. 1995), 297–309.

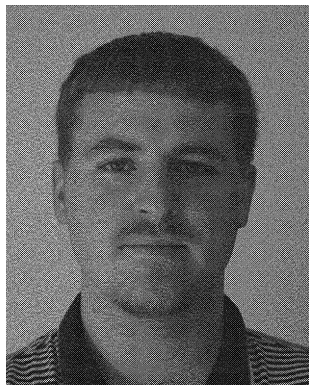
- [3] Gerlach, K. (2002) Outlier resistant adaptive matched filters. *IEEE Transactions on Aerospace and Electronic Systems*, **38**, 2 (July 2002), 885–901.
- [4] Chen, P., Melvin, W. L., and Wicks, M. C. (1999) Screening among multivariate normal data. *Journal of Multivariate Analysis*, **69** (1999), 10–29.
- [5] Rabideau, D. J., and Steinhardt, A. O. (1996) Improving the performance of adaptive arrays in nonstationary environments through data-adaptive training. In *Proceedings of the 30th Asilomar Conference on Signal, Systems and Computers*, Pacific Grove, CA, Nov. 3–6, 1996.
- [6] Melvin, W. L., Wicks, M. C., and Brown, R. D. (1996) Assessment of multichannel airborne radar measurements for analysis and design of space-time processing architectures and algorithms. In *Proceedings of the 1996 IEEE National Radar Conference*, Ann Arbor, MI, May 13–16, 1996, 130–135.
- [7] Richmond, C. D. (2000) Performance of a class of adaptive detection algorithms in nonhomogeneous environments. *IEEE Transactions on Signal Processing*, **48**, 5 (May 2000), 1248–1262.
- [8] Rabideau, D. J., and Steinhardt, A. O. (1999) Improved adaptive clutter cancellation through data-adaptive training. *IEEE Transactions on Aerospace and Electronic Systems*, **35** (July 1999), 879–891.
- [9] Melvin, W. L., and Wicks, M. C. (1997) Improving practical space-time adaptive radar. In *1997 IEEE National Radar Conference Record*, 48–53.
- [10] Richmond, C. D. (1998) Response of sample covariance based MVDR beamformer to imperfect look and inhomogeneities. *IEEE Signal Processing Letters*, **5**, 12 (1998), 325–327.
- [11] Rangaswamy, M., Himad, B., and Michels, J. H. (2001) Performance analysis of the nonhomogeneity detector for STAP applications. In *2001 National Radar Conference Record*, 193–197.
- [12] Kreithen, D. E., and Steinhardt, A. O. (1996) Target detection in post-STAP undernulled clutter. In *Proceedings of the 29th Asilomar Conference on Signals, Systems, and Computers*, Vol. 2, 1996, 1203–1207.
- [13] Maher, J., Callahan, M., and Lynch, D. (2000) Effects of clutter modeling in evaluating STAP processing for space-based radars. In *Proceedings of IEEE International Radar Conference 2000*, 565–570.
- [14] Horn, R., and Johnson, C. (1983) *Matrix Analysis*, New York: Cambridge University Press, 1983.
- [15] Steiner, M. J., and Gerlach, K. (1998) Fast-converging maximum-likelihood adaptive signal processing. In *1998 IEEE National Radar Conference Record*, 117–122.
- [16] Steiner, M. J., and Gerlach, K. (2000) Fast converging adaptive canceller for a structured covariance matrix. *IEEE Transactions on Aerospace and Electronic Systems*, **36**, 4 (Oct. 2000), 1115–1126.
- [17] McWhorter, L. T., and Scharf, L. L. (1996) Adaptive matched subspace detectors and adaptive coherence. In *Proceedings of 30th Asilomar Conference on Signals, Systems, Vol. 2*, Los Alamitos, CA, Nov. 1996, 1114–1117.
- [18] Pulsone, N. B., and Zatman, M. A. (2000) A computational efficient two-step implementation of the GLRT. *IEEE Transactions on Signal Processing*, **48**, 3 (Mar. 2000), 609–616.
- [19] DiFranco, J. V., and Rubin, W. L. (1980) *Radar Detection*. Dedham, MA: Artech House, 1980.
- [20] Carlson, B. D. (1988) Covariance matrix estimation errors and diagonal loading in adaptive arrays. *IEEE Transactions on Aerospace and Electronic Systems*, **24**, 4 (1988), 397–401.
- [21] Haimovich, A. M., and Bar-Ness, Y. (1991) An eigenanalysis interference canceller. *IEEE Transactions on Signal Processing*, **39**, 1 (Jan. 1991), 76–84.
- [22] Yu, J.-L., and Yeh, C.-C. (1995) Generalized eigenspaced-based beamformers. *IEEE Transactions on Signal Processing*, **43** (Nov. 1995), 2453–2461.
- [23] Picciolo, M. L., and Gerlach, K. (2001) Fast converging robust adaptive arrays. In *Proceedings 2001 IEEE Radar Conference*, Atlanta, GA, May 1–3, 2001, 216–221.
- [24] Picciolo, M. L., Gerlach, K., and Goldstein, J. S. (2002) An adaptive multistage median cascaded canceller. In *Proceedings of 2002 IEEE Radar Conference*, Long Beach, CA, Apr. 22–25, 2002, 318–325.
- [25] Picciolo, M. L., and Gerlach, K. (2003) A median cascaded canceller for robust adaptive array processing. *IEEE Transactions on Aerospace and Electronic Systems*, **39**, 3 (July 2003), 883–900.
- [26] Ward, J. (1994) Space-time adaptive processing for airborne radar. Technical report 1015, Lincoln Laboratory, Dec. 1994.
- [27] Kirsteins, I. P., and Tufts, D. W. (1994) Adaptive detection using low rank approximation to a data matrix. *IEEE Transactions on Aerospace and Electronic Systems*, **30**, 1 (Jan. 1994), 55–67.
- [28] Kirsteins, I. P., and Tufts, D. W. (1991) Rapidly adaptive nulling of interference. In Bouvet and Bienvenu (Eds.), *High Resolution Methods in Underwater Acoustics*, New York: Springer-Verlag, 1991.
- [29] Brennan, L. E., and Reed, I. S. (1973) Theory of adaptive radar. *IEEE Transactions on Aerospace and Electronic Systems*, **AES-9**, 2 (Mar. 1973), 237–252.
- [30] Bergin, J. S., and Techau, P. M. (2002) High-fidelity site-specific radar simulations: KASSPER '02 workshop datacube. ISL Technical report ISL-SCRD-TR-02-105, Vienna, VA, May, 2002.
- [31] Babu, B. N. S., Torres, J. A., and Melvin, W. L. (1996) Processing and evaluation of multichannel airborne radar measurements (MCARM) measured data. In *IEEE International Symposium on Phased Array Systems and Technology*, 1996, 395–399.



Karl Gerlach (M'81—F'02) was born in Chicago, IL. He received his B.S. in 1972 from the University of Illinois, Urbana, and his M.S. and D.Sc. from George Washington University, Washington, D.C., in 1975 and 1981, respectively, all in electrical engineering.

Since 1972, he has been employed by the Naval Research Laboratory in Washington, D.C. From 1972 to 1976, he worked on experimental submarine communications systems and from 1976 to the present he has been with the Radar Division where his research interests include adaptive signal processing and space-based radar.

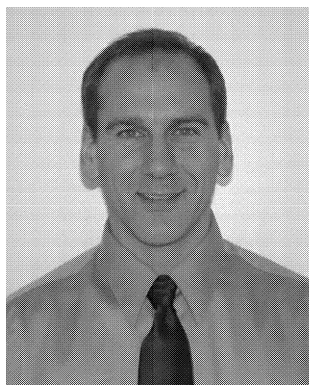
Dr. Gerlach was the 1986 recipient of the IEEE AESS Radar Systems Panel award.



Shannon D. Blunt (S'96—M'02) received the B.S., M.S., and Ph.D. degrees in electrical engineering in 1999, 2000, and 2002, respectively, from the University of Missouri—Columbia (MU).

He is currently with the Radar Division of the U.S. Naval Research Laboratory, Washington, D.C. His research interests are in adaptive signal processing for radar and communications with a current emphasis on waveform diversity techniques.

Dr. Blunt received the Donald K. Anderson Graduate Student Teaching award in Electrical Engineering from MU in 2000 and the MU Outstanding Graduate Student award in Electrical Engineering in 2001. He is a member of Eta Kappa Nu and Tau Beta Pi.



Michael L. Picciolo (S'87—M'88—SM'00) received a B.S. from Clarkson University, Potsdam, NY in 1988, an M.S. from Catholic University, Washington, D.C. in 1993, and a Ph.D. from Virginia Tech (Northern VA campus) in 2003, all in electrical engineering.

He currently works for SAIC in Chantilly, VA as an adaptive signal processing analyst. From 1988–2003 he worked for the Radar Division of the U.S. Naval Research Laboratory, Washington, D.C. He designed next generation surveillance radar systems and created novel adaptive signal processing algorithms. His interests include the field of robust statistics and the design of robust, fast-converging, adaptive algorithms. Application areas have included space-time adaptive processing (STAP) in airborne radar systems, advanced shipboard adaptive phased array radars, and radar sidelobe cancellers.

Dr. Picciolo serves as chair of the IEEE Signal Processing chapter, Northern Virginia Section (1999–present), and also as the section treasurer for 2003.